On the Path-Dependence of the *J*-integral Near a Stationary Crack in an Elastic-Plastic Material

Dorinamaria Carka and Chad M. Landis*
The University of Texas at Austin, Department of Aerospace Engineering and Engineering Mechanics, 210 East 24th Street, C0600, Austin, TX 78712-0235

Abstract

The path-dependence of the *J*-integral is investigated numerically, via the finite element method, for a range of loadings, Poisson's ratios, and hardening exponents within the context of J_2-flow plasticity. Small-scale yielding assumptions are employed using Dirichlet-to-Neumann map boundary conditions on a circular boundary that encloses the plastic zone. This construct allows for a dense finite element mesh within the plastic zone and accurate far-field boundary conditions. Details of the crack tip field that have been computed previously by others, including the existence of an elastic sector in Mode I loading, are confirmed. The somewhat unexpected result is that J for a contour approaching zero radius around the crack tip is approximately 18% lower than the far-field value for Mode I loading for Poisson's ratios characteristic of metals. In contrast, practically no path-dependence is found for Mode II. The applications of T or S stresses, whether applied proportionally with the K-field or prior to K, have only a modest effect on the path-dependence.

Keywords: elasto-plastic fracture mechanics, small scale yielding, path-dependence of the *J*-integral, finite element methods

1. Introduction

The *J*-integral as introduced by Eshelby [1,2] and Rice [3] is perhaps the most useful quantity for the analysis of the mechanical fields near crack tips in both linear elastic and non-linear elastic materials. For non-linear elastic materials it is well known that the *J*-integral is equivalent to the energy release rate, [1-3]. Additionally, J has been used in several studies to characterize the intensity of the stress and deformation fields near cracks in power-law hardening materials, [3-8]. It is established that J is a path-independent integral when the material is non-linear elastic [3,4]. As such, the path independence of J rigorously holds in elastic-plastic materials when the material response is governed by the deformation theory of plasticity, or when flow theory exactly mimics deformation theory (where proportional loading occurs at all points within the domain). Rice [4,9] has demonstrated that, in fact, flow theory plasticity does perfectly mimic deformation theory near a stationary crack tip loaded in mode III in an elastic-power-law hardening material under small scale yielding conditions. Hence

* landis@mail.utexas.edu, phone 512-471-4273, fax 512-471-5500,
210 East 24th Street, C0600, Austin, TX 78712-0235

for mode III, the J-integral is path-independent for small scale yielding. No such proof of the path-independence of J is available for the in-plane loading modes, and we will show that J is not path-independent in cases with a mode I component.

In any situation where a significant amount of non-proportional loading occurs it is expected that the J-integral will not be path-independent. For example, McMeeking [10] analyzed the effects of finite deformation near a mode I crack and found that the blunting of the crack tip causes unloading which results in the path-dependence of J. Rice and Sorenson [11] and Drugan et al. [12] have shown that for steadily growing cracks, where there is a significant amount of non-proportional straining including elastic unloading and plastic reloading, the strain singularity in an elastic-perfectly-plastic material is $\sim \ln(1/r)$ and hence J evaluated around a contour close to the crack tip is zero. However, in this work we do not consider the effects of finite deformation and the crack tip remains stationary, yet J is found to be path-dependent. Since proportional loading is not guaranteed for in-plane loading the finding that J is path-dependent is not entirely unexpected, however the amount of path-dependence is an unforeseen result.

We now proceed to the description of the material constitutive model. Power-law hardening materials as described by Rice and Rosengren [5] are studied such that the uniaxial stress-strain behavior is described by,

$$\begin{aligned} \frac{\sigma}{\sigma_0} &= \frac{\varepsilon}{\varepsilon_0} \quad \text{for } \varepsilon \le \varepsilon_0 \\ \frac{\sigma}{\sigma_0} &= \left(\frac{\varepsilon}{\varepsilon_0}\right)^N \quad \text{for } \varepsilon \ge \varepsilon_0 \end{aligned} \,. \tag{1.1}$$

The initial yield strength is σ_0, and the uniaxial strain at initial yield is ε_0. These material parameters are related through the Young's modulus, E, as $\sigma_0 = E\varepsilon_0$. The strain hardening exponent is N, with $N = 0$ representing perfect plasticity and $N = 1$ linear elasticity. The J_2-flow theory of plasticity is used for the multi-axial generalization of the material constitutive response such that the increments of the Cartesian stress tensor components, $d\sigma_{ij}$, are given as,

$$d\sigma_{ij} = \frac{E\nu}{(1+\nu)(1-2\nu)} d\varepsilon_{kk}\delta_{ij} + \frac{E}{1+\nu}(d\varepsilon_{ij} - d\varepsilon^p_{ij}). \tag{1.2}$$

Here, the Poisson's ratio is ν, δ_{ij} is the Kronecker delta, and the Cartesian components of the total strain and plastic strain increments are $d\varepsilon_{ij}$ and $d\varepsilon^p_{ij}$. Throughout this paper standard Einstein notation is used with summation over repeated indices

assumed. Within the context of J_2-flow theory, the plastic strain increments are proportional to the stress deviator components, $s_{ij} = \sigma_{ij} - \sigma_{kk}\delta_{ij}/3$,

$$d\varepsilon_{ij}^{p} = \frac{3}{2}\frac{d\overline{\varepsilon}^{p}}{\overline{\sigma}} s_{ij} \,. \tag{1.3}$$

Here the effective uniaxial stress is $\overline{\sigma} = \sqrt{\frac{3}{2} s_{ij} s_{ij}}$, and the effective uniaxial strain increment is $d\overline{\varepsilon}^{p} = \sqrt{\frac{2}{3} d\varepsilon_{ij}^{p} d\varepsilon_{ij}^{p}}$. During continued plastic deformation the stress state is constrained to reside on the yield surface given by,

$$\tfrac{3}{2} s_{ij} s_{ij} = \sigma_{y}^{2} \,. \tag{1.4}$$

The current level of the yield strength, σ_{y}, satisfies the following nonlinear equation in order to be consistent with the uniaxial behavior described by Equation (1.1),

$$\frac{\overline{\varepsilon}^{p}}{\varepsilon_{0}} = \left(\frac{\sigma_{y}}{\sigma_{0}}\right)^{1/N} - \frac{\sigma_{y}}{\sigma_{0}} \,, \tag{1.5}$$

where the total effective plastic strain is simply the sum of all increments, $\overline{\varepsilon}^{p} = \int d\overline{\varepsilon}^{p}$, throughout the history of loading.

The study of the path-dependence of the J-integral will take place within the context of the small scale yielding boundary layer approach as described by Rice [3,4,13]. A semi-infinite crack with crack flanks along the negative x-axis and crack tip located at the origin is studied. At sufficiently remote distances from the crack tip, the fields are governed by linear elasticity and the stresses approach the combined K-T field given as,

$$\begin{Bmatrix} \sigma_{xx} \\ \sigma_{yy} \\ \sigma_{xy} \end{Bmatrix} = \frac{K_{\mathrm{I}}}{\sqrt{2\pi r}} \cos\tfrac{\theta}{2} \begin{Bmatrix} 1 - \sin\tfrac{\theta}{2}\sin\tfrac{3\theta}{2} \\ 1 + \sin\tfrac{\theta}{2}\sin\tfrac{3\theta}{2} \\ \sin\tfrac{\theta}{2}\cos\tfrac{3\theta}{2} \end{Bmatrix} + \frac{K_{\mathrm{II}}}{\sqrt{2\pi r}} \begin{Bmatrix} \sin\tfrac{\theta}{2}(-2 + \cos\tfrac{\theta}{2}\cos\tfrac{3\theta}{2}) \\ \sin\tfrac{\theta}{2}\cos\tfrac{\theta}{2}\cos\tfrac{3\theta}{2} \\ \cos\tfrac{\theta}{2}(1 - \sin\tfrac{\theta}{2}\sin\tfrac{3\theta}{2}) \end{Bmatrix} + \begin{Bmatrix} T \\ 0 \\ 0 \end{Bmatrix} . \tag{1.6}$$

The coefficients K_{I}, K_{II}, and T are the mode I and mode II stress intensity factors, and the magnitude of the T-stress respectively. In the out-of-plane direction generalized plane strain is imposed such that the out-of-plane axial strain is constant throughout the domain and given by,

$$\varepsilon_{zz} = \frac{1}{E}(S - \nu T)\,, \tag{1.7}$$

with S as the far field out-of-plane axial stress σ_{zz}.

Neglecting the S and T stresses, the characteristic size of the plastic zone around the crack tip is approximated as,

$$R_p = \frac{1}{3\pi}\frac{K_{\mathrm{I}}^2 + \frac{25}{4}K_{\mathrm{II}}^2}{\sigma_0^2}\,. \tag{1.8}$$

Using this mixed-mode definition of the plastic zone size, the maximum radial distance from the crack tip to the perimeter of the yielded region in an elastic-perfectly-plastic material is $R_{\max} \approx 1.4R_p$ for all combinations of K_{I} and K_{II}. Details of the shapes of the plastic zones for perfect plasticity are shown in Figure 1. The next section is devoted to the numerical solution procedure applied for the calculation of the fields and the J-integral.

2. Numerical methods

The calculation of the fields and the resulting path-dependence of the J-integral is carried out by separating the x-y plane into two regions, a small circular region of radius R that must encompass the entire plastic zone and the remainder of the plane composed of linear elastic material. For the computations to be presented in this paper, the final plastic zone size, R_p, is approximately one half of R. The inner circular region is represented by a radial mesh of 9-noded isoparametric elements with 4-point reduced integration for the hydrostatic strains, and full 9-point integration for the deviatoric strains. The arc subtended by each element is $\pi/25$, and the radial length of the elements varies from $R/400$ for the first ring of elements around the crack tip to $R/20$ for the last ring. For perfect plasticity, when $N = 0$, the crack tip elements are triangular elements created by collapsing one side of the 9-noded quadrilaterals and giving each of the crack tip nodes separate degrees of freedom. We have found that, for perfect plasticity, moving the mid-side nodes along the rays to the quarter-points as suggested by Barsoum [14] is inferior to keeping them at the midpoint. This is likely due to the fact that the $1/\sqrt{r}$ strain field that exists in the quarter-point elements corrupts the $1/r$ singular strain field. In fact, we were not able to obtain mode II solutions for perfect plasticity with the quarter-point elements. The quarter-point elements are used, and provide very accurate results, for the linear elastic cases. For the strain hardening cases the special 6-noded singular triangular elements developed by Stern [15] are implemented around the crack tip.

The region $r > R$ is represented by a Dirichlet to Neumann map for a semi-infinite crack. The full derivation of these boundary conditions is given in Carka *et al.* [16], which builds upon prior work of Givoli and co-workers [17,18] and Hilton and Hutchinson [19]. The basic idea is that the region $r > R$ adds both stiffness contributions and forces associated with the K-T field to the boundary of the finite element mesh. The finite element connectivity of the infinite region stiffness mimics a super-element with stiffness interactions between each of the degrees of freedom on the arc $r = R$. However, if the node numbering of the finite element region proceeds first in the angular coordinate and then in the radial coordinate, the overall bandwidth of the full stiffness matrix is not increased by the fully-dense contribution of the infinite region stiffness. Ultimately these boundary conditions allow for a very dense mesh in the plastic zone with no degrees of freedom expended by attempting to model the infinite region with a large but finite domain. Furthermore, no finite size approximation, imposed by applying either traction or displacement boundary conditions at a finite radial distance, is needed to represent the far-field loading since the true infinite boundary conditions are enforced to within the same accuracy as the angular discretization on the arc $r = R$ allows. Landis [20] used similar boundary conditions to study mode III and analogous electrical mode E crack tip fields, and has shown that this numerical approach provides highly accurate agreement with the analytical results due to Rice [9].

Following the successful solution of the mechanical fields for a given combination of applied loading and material properties, the J-integral is computed along several circular arcs of different radii. The J-integral is calculated with the domain integral method of Li *et al.* [21]. The derivation by Li et al. [21] is strictly valid only for non-linear elastic materials where the J-integral is path-independent, and not for materials obeying flow theory where non-proportional loading is present and J is path-dependent. However, the domain integral method is still valid for obtaining the radial average of J over the domain. The proof of this statement is as follows. First, the definition of J for a counterclockwise path Γ encircling the crack tip is [3,4],

$$J = \int_{\Gamma} \left(W n_1 - \sigma_{ji} n_j u_{i,1} \right) d\Gamma \,, \tag{2.1}$$

where n_i are the Cartesian components of the outward unit normal to the path, $u_{i,j}$ are the Cartesian components of the displacement gradient, and W is the integrated material work density, $W = \int \sigma_{ij} \, d\varepsilon_{ij}$. Consider the associated domain integral introduced by Li *et al.* [21].

$$J_A = -\int_A \left(W q_{,1} - \sigma_{ji} q_{,j} u_{i,1} \right) dA \tag{2.2}$$

Here A is an area that contains both the top and bottom crack faces as part of its boundary. For our specific calculations A will be a circular annulus with inner radius R_i and outer radius R_o. For nonlinear elastic materials J is path-independent and $J_A = J$ for any q that is unity along the inner boundary of A and zero along its outer boundary. For the present radial average proof the function q must be,

$$q = \frac{r - R_o}{R_i - R_o} \rightarrow q_{,j} = \frac{r_{,j}}{R_i - R_o} = \frac{n_j}{R_i - R_o}. \tag{2.3}$$

Substituting (2.3) into (2.2) we obtain,

$$J_A = -\int_A \left(W q_{,1} - \sigma_{ji} q_{,j} u_{i,1} \right) dA = \frac{1}{R_o - R_i} \int_{R_i}^{R_o} \left[\int_{-\pi}^{\pi} \left(W n_1 - \sigma_{ji} n_j u_{i,1} \right) r \, d\theta \right] dr, \tag{2.4}$$

and hence J_A is the radial average of J over all circular paths between R_i and R_o. Therefore, when $J(r)$ is reported using a domain integral, r is taken as the average of R_i and R_o.

For any path Γ that does not pass through any part of the plastic zone it can be proven that the J-integral is equal to,

$$J_\infty = \frac{1 - \nu^2}{E} \left(K_{\mathrm{I}}^2 + K_{\mathrm{II}}^2 \right). \tag{2.5}$$

In the following section results will be reported for the shapes of the plastic zones, the stresses near the crack tip, and for the radial variation of the J-integral. Dimensional analysis can be used to prove that normalized quantities like σ_{ij} / σ_0, $\varepsilon_{ij} / \varepsilon_0$, and J / J_∞ are independent of the ratio of σ_0 / E, and hence the path-dependence of J only needs to be investigated over the following parameter space,

$$\frac{J(r / R_p)}{J_\infty} = f(\nu, N, \psi, T / \sigma_0, S / \sigma_0) \tag{2.6}$$

where

$$\psi = \arctan\left(\frac{K_{\mathrm{II}}}{K_{\mathrm{I}}} \right). \tag{2.7}$$

Results over a limited range of this parameter space are presented next.

3. Results

The first set of results presented in Figure 1 are the shapes of the plastic zones for mode I, mode II, and mixed mode loading with $K_{\mathrm{I}} = K_{\mathrm{II}}$ for an elastic-perfectly-plastic material with $\nu = 0.3$, and $S = T = 0$. The size of the plastic zones is dictated by the magnitudes of the intensity factors and is given specifically by Equation (1.8). Note that the factor of 25/4 multiplying the K_{II} contribution to R_p indicates that the mode II plastic zone size is significantly larger than the mode I zone for equivalent levels of the intensity factors. Also note that the addition of hardening to the calculations does change the size and shape of the plastic zones. Our numerical results for the effect of N on the plastic zone are very similar to those shown in [7].

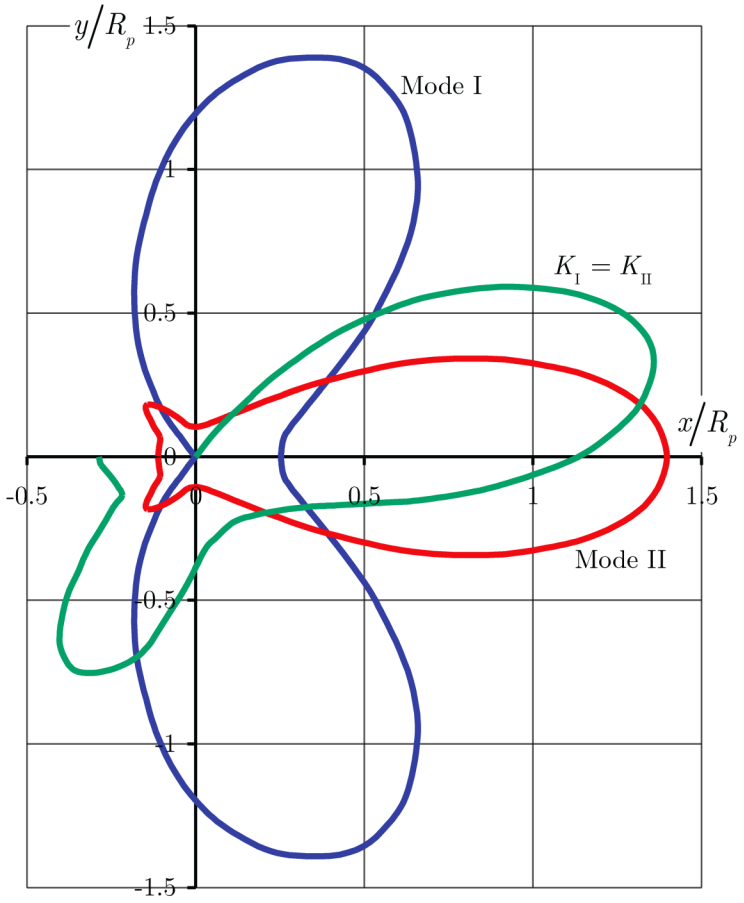

Figure 1. Plastic zone shapes for mode I (blue), mode II (red), and mixed mode loading with $K_{\mathrm{I}} = K_{\mathrm{II}}$ (green) for an elastic-perfectly-plastic material with $\nu = 0.3$, and $S = T = 0$.

As observed by Rice and Tracey [22], and Du and Hancock [23], the mode I plastic zone does not entirely surround the crack tip. Our calculations indicate that the elastic sectors extend from $-180^\circ \le \theta < -148^\circ$ and $148^\circ \le \theta < 180^\circ$. Given the differences in mesh density, this result is in agreement with these prior studies (recall that the arc covered by each element is 7.2° in this work). Calculations implementing the J_2-deformation theory of plasticity have also been performed and show that while the overall shape of the plastic zone is similar to that from flow theory, the elastic sector on the crack flanks does not exist. Computations for pure Mode II indicate that the plastic zones predicted from the flow and deformation theories are nearly indistinguishable from one another. An additional comparison between flow theory and deformation theory is

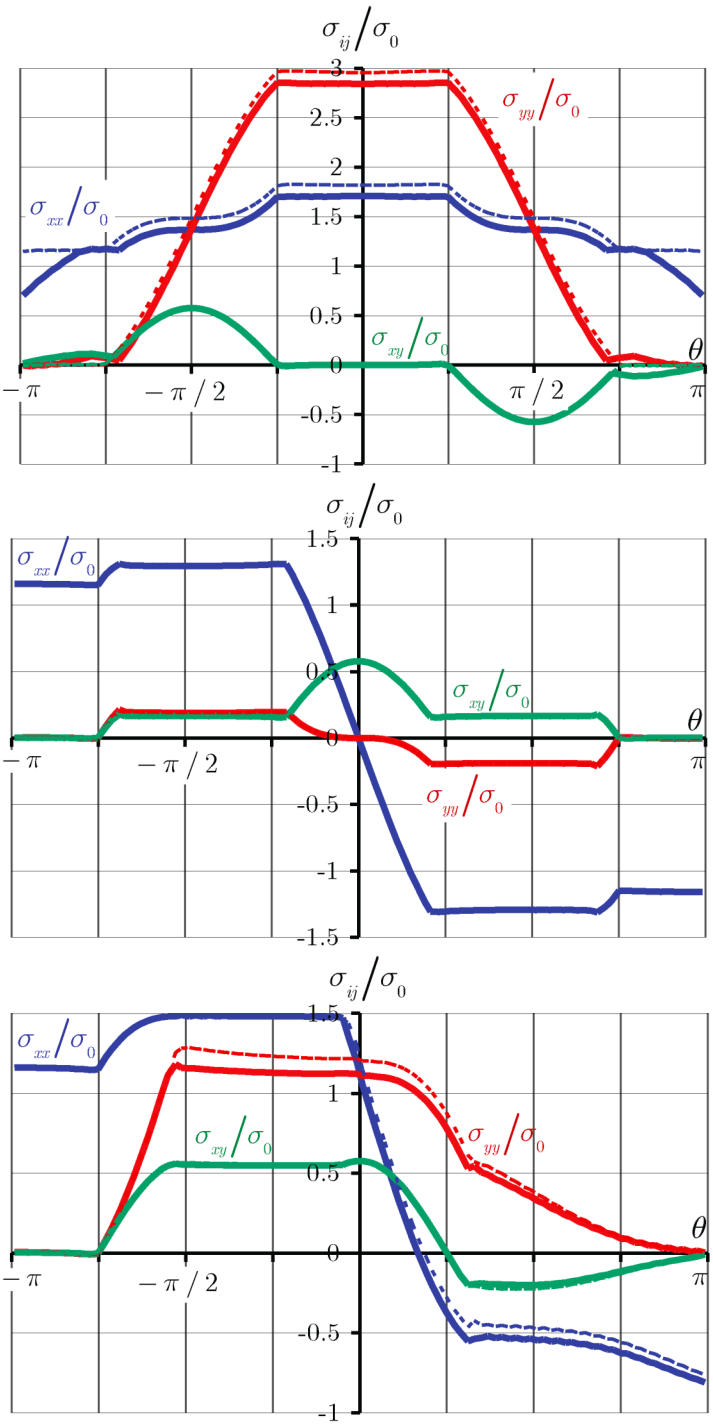

Figure 2. Angular variations of the Cartesian components of the stress around a crack tip in an elastic-perfectly-plastic material with $\nu = 0.3$, and $S = T = 0$ for (a) mode I, (b) mode II, and (c) $K_{\mathrm{I}} = K_{\mathrm{II}}$. Solid lines are the solutions for flow theory and dashed lines are for deformation theory.

shown in Figure 2. Figure 2 plots the angular distribution of stresses near the crack tip for the same cases studied in Figure 1. In each of these figures the solid lines correspond to flow theory and the dashed lines to deformation theory. Figure 2a shows that for mode I the deformation theory results follow the Prandtl crack tip field perfectly, while the flow theory results differ from the Prandtl field throughout the entire angular range. We find that the flow theory results for the axial stress in the constant stress sector ahead of the crack tip is $\sigma_{yy} = 2.85\sigma_0$ when $\nu = 0.3$ and $\sigma_{yy} = 2.89\sigma_0$ when $\nu = 0.49$, as compared to the values of $2.96\sigma_0$ and $2.90\sigma_0$ when $\nu = 0.3$ computed by Rice and Tracey [22] and Du and Hancock [23] respectively. For deformation theory our computed result for stress ahead of the crack tip is $\sigma_{yy} = 2.97\sigma_0$, which is in nearly perfect agreement with the Prandtl slip-line field prediction. In contrast, the flow and deformation theory results for mode II are practically identical to one another, as the dashed lines for the deformation theory results are hidden by the solid flow theory curves. Finally, as for the mode I results, the mixed mode case shows a difference between the flow and deformation theories. Note however, that for this case the two theories are coincident near the

crack flank that bounds the plastic zone. Given that the J-integral is path-independent for flow theory plasticity only in the cases where it mimics deformation theory, i.e. for proportional loading at all points in the plastic zone, these results suggest that the most significant cases of path-dependence should occur under predominantly mode I loading.

Figure 3 illustrates the primary and perhaps the most intriguing result of this paper. Here, the path-dependence of the J-integral for mode I loading on an elastic-perfectly-plastic material with $\nu = 0.3$, and $S = T = 0$ is demonstrated. Included on this plot are results from four different K_{I} levels from the same simulation corresponding to plastic zone sizes that are 12.5, 50, 112.5, and 200 times the radial dimension of the first ring of elements surrounding the crack tip, $h^r_{\min}$. The loading to the final K_{I} level is broken into 400 equal increments, such that these plastic zone sizes result from 100, 200, 300 and 400 load steps respectively. The results in Figure 3 demonstrate several features of the present numerical solution. First, self-similarity of the solution is achieved even when the plastic zone is relatively small compared to the finite element mesh size.

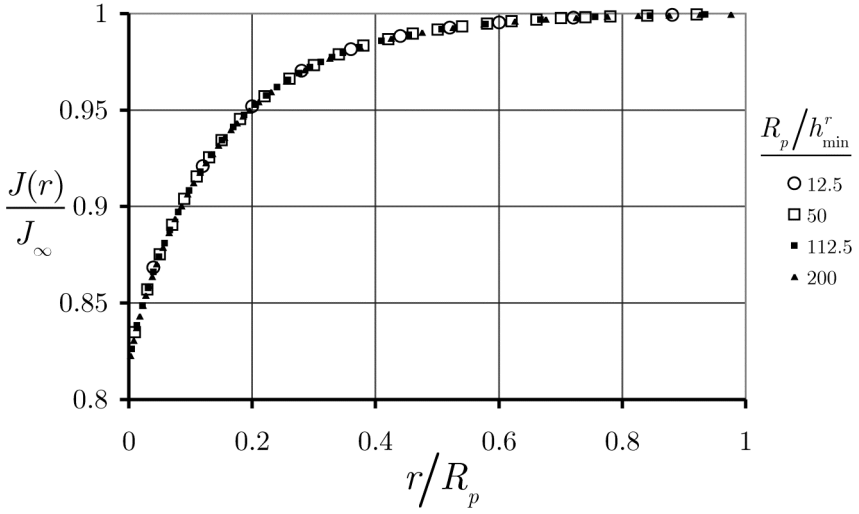

Figure 3. Values for the J-integral for a circular contour of radius r computed by the domain integral method near a crack tip under mode I loading in an elastic-perfectly-plastic material with $\nu = 0.3$. The markers correspond to different points along the load history and different sizes of the plastic zone relative to the minimum radial dimension of the elements surrounding the crack tip.

A second test of the self-similarity of the solution is on the normalized crack tip opening displacement, $\delta_t \sigma_0 / J_\infty$. For this calculation with $\nu = 0.3$, we find that $\delta_t \sigma_0 / J_\infty = 0.61$ after the full 400 load steps, and that this normalized quantity is larger than 0.61 by 10% and 1% after 14 and 81 load steps respectively. Hence again, self-similarity of the numerical solution is achieved after approximately 100 of the 400 load steps to within a 1% level of convergence. For comparison, the numerical results obtained by Rice and Tracey [22] and Levy et al. [24] are $\delta_t \sigma_0 / J_\infty = 0.54$ and 0.47 respectively, and an approximation due to Rice [3] is $\delta_t \sigma_0 / J_\infty = 0.67$. Note that the quality of the self-similarity of the present results is a testament to the utility and

accuracy of the infinite boundary conditions that have been implemented. The second feature of the numerical solution displayed in Figure 3 is the convergence of the results with respect to both mesh density and load increment refinement. Here, both mesh density with respect to the plastic zone size and the load increments are effectively refined as the loading progresses. We have also studied the convergence of the solution by fixing the mesh density and increasing the number of load increments, and by fixing the number of load increments and increasing the mesh density. In both cases we find the same features that are shown in Figure 3. Specifically, increasing either the mesh density or the number of load increments *increases* the computed level of J path-dependence, i.e. the J/J_∞ results converge to their final results from above. The linearly extrapolated J/J_∞ values at $r=0$ are 0.842, 0.824, 0.820, and 0.819 for $R_p/h^r_{\min}$ equal to 12.5, 50, 112.5, and 400 respectively. Finally, note that since the largest radial extent of the plastic zone is approximately $1.4R_p$ the J contour on $r=R_p$ actually passes through the plastic zone. At $r=R_p$ these calculations show that $J=0.9997J_\infty$. For all of the contours outside of the plastic zone the calculated J is less than 0.01% *above* the theoretical value of Equation (2.5).

We find that for $\nu=0.3$, J evaluated along a contour of zero radius about the crack tip is 18% lower than its far field value. The next sets of results illustrate the effects of the hardening exponent and the mode-mix on the path-dependence of J, again for $\nu=0.3$ and $S=T=0$. With regard to the hardening exponent it is well known that J must be path-independent for $N=1$, which corresponds to a linear elastic material. This is in fact what the numerical results presented in Figure 4 show, with $\Delta J/J_\infty$ decreasing monotonically from 18% for perfect plasticity to 0 for linear elastic behavior. Also displayed on Figure 4 is the effect of mode-mix on the path-dependence. Here $\cos\psi=0$ corresponds to pure mode II and $\cos\psi=1$ is pure mode I. The stress and strain fields for pure mode II have been analyzed to determine if proportional loading occurs at all points in the plastic zone, and this was found *not* to be the case. Hence, this finding does not suggest that $\Delta J/J_\infty$ should be zero in this case, however, at least to within the accuracy of the

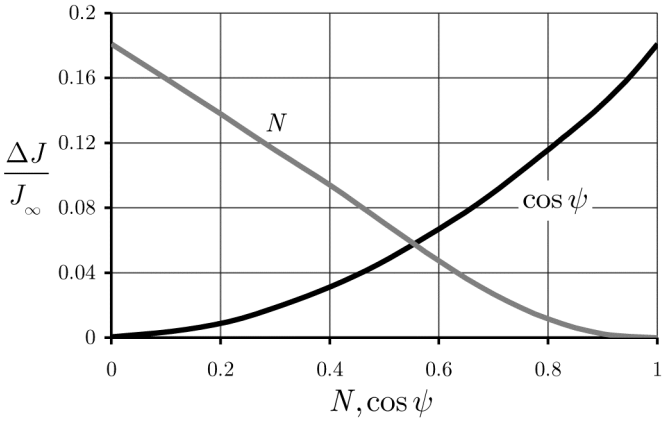

Figure 4. The effects of the strain hardening exponent in mode I and the mode-mix for perfect plasticity on the relative decrease in J at the crack tip. As for the previous results $\nu=0.3$ and

present numerical results, it is not possible to claim that $\Delta J / J_\infty$ is not equal to zero for pure mode II loading.

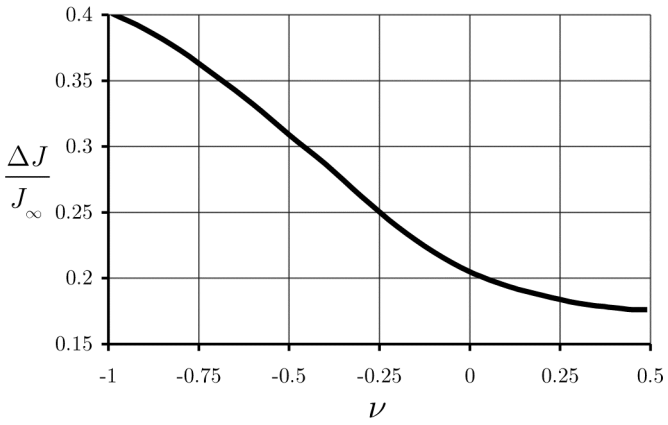

Figure 5. The effects of Poisson's ratio on the relative decrease in J at the crack tip for pure mode I loading in an elastic-perfectly-plastic material.

As mentioned previously, it is possible to prove through dimensional analysis that the ratio σ_0 / E has no effect on the results for the path-dependence of J, and this has been verified numerically as well. However, the Poisson's ratio does have a mild effect on $\Delta J / J_\infty$ for $\nu > 0$ and a much more marked effect for $\nu < 0$. Figure 5 plots the relative decrease in J at the crack tip with respect to the far field value for mode I loading and $S = T = 0$ over the full range of Poisson's ratios in an elastic-perfectly-plastic material. $\Delta J / J_\infty$ ranges from 17.5% when $\nu = 0.49$, to 20.5% at $\nu = 0$, and finally to 39.5% at $\nu = -0.99$. Therefore, for properties characteristic of most ductile metals, Poisson's ratio has little effect on the value of $\Delta J / J_\infty$ which is close to 18% for $0.1 < \nu < 0.4$.

The final investigation to be presented is on the effects of the T and S-stresses. Du and Hancock [23] performed a detailed study of the effects of the T-stress on the crack-tip constraint, and Rice [13] has commented on issues associated with neglecting T-stresses. Overall, our computations confirm Du and Hancock's results about the effects of T on the extent of the elastic sector and the sizes and shapes of the plastic zones. Here, we also investigate the effects of the non-singular S-stress (the far field σ_{zz} component of the stress tensor), and again our focus is on the path-dependence of J. Note that for the mixed-mode loadings shown in Figure

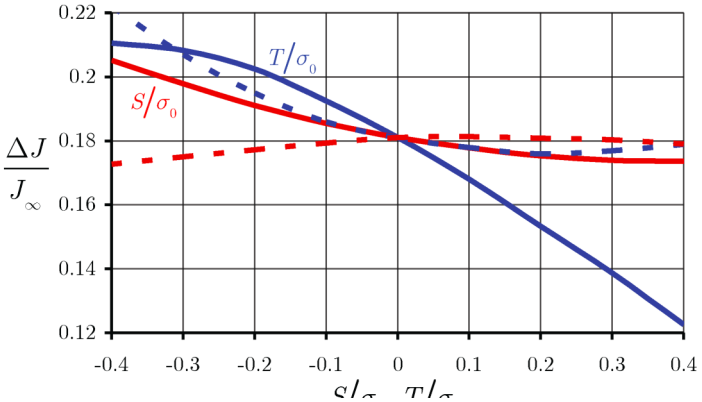

Figure 6. The effects of the non-singular S and T-stresses on the relative decrease in J at the crack tip for pure mode I loading in an elastic-perfectly-plastic material with $\nu = 0.3$. The red curves correspond to the existence of S with T=0, and the blue curves are for nonzero T with S=0. The dashed lines represent solutions when the non-singular stresses are applied proportionally with K_I, and the solid curves are for when S or T is applied prior to K_I.

4, $K_{\rm I}$ and $K_{\rm II}$ were applied proportionally. For the T and S-stresses, we have studied both a proportional application of the transverse stresses with the K-field, as well as applying the transverse stress prior to the application of $K_{\rm I}$. The proportional loading study is motivated by a monotonic loading of a specimen with an arbitrary three-dimensional geometry and loading with mode I symmetry. In such cases T, S and $K_{\rm I}$ are each proportional to the loading parameter and are thus proportional to one another throughout the loading. One issue that results from this type of loading is that the solution for the fields is not self-similar. For very small applied loadings the non-singular stresses are close to zero, but the K-field persists and produces a plastic zone like the one illustrated in Figure 1. However, as the load is increased the S and T-stresses grow and have a significant and ever-changing impact upon the plastic zone size and shape, the overall field distributions, and the path-dependence of the J-integral. In contrast, if the non-singular stresses are applied prior to the K-field loading, then self-similarity is maintained with the plastic zone and associated fields growing into an unvarying loaded environment. The results for the path-dependence of J for either S or T acting in the absence of the other are shown in Figure 6. Overall the effect of the non-singular stresses is relatively mild with compressive/tensile stresses tending to increase/decrease the amount of path-dependence (although the reverse occurs in the case of a proportionally applied S-stress).

4. Discussion

It is noteworthy that several pioneering researchers in the field of non-linear fracture mechanics have made very careful remarks about the path-independence of the J-integral in the context of flow theory plasticity, [4-6,8,9,22-24]. However, a quantitative determination of the path-dependence of J under in-plane loading conditions has not appeared. This manuscript has attempted to fill that gap with accurate numerical analyses. Several of the results presented in this work are in rough quantitative agreement with prior works. Additionally, in *all* of the cases presented here for flow theory, we have also performed the corresponding deformation theory calculations and have found J to be in agreement with the theoretical value of Equation (2.5) to within 0.1% for all paths, including the ring of elements in contact with the crack tip. Hence, our numerical methods yield accurate results for J in the case of deformation theory where path-independence is a rigorously proven result. Finally, there is one other numerical study, [24], where it was noticed that the strength of the strain singularity near the crack tip was smaller than approximations based upon deformation theory plasticity. Their rough approximation of the effect on the crack tip value of J was a 25% reduction, which is certainly in qualitative agreement with the present result of 18%.

Acknowledgement
This work has been supported by the Army Research Office contract #W911NF-07-1-0495.

References

1. Eshelby, J.D., "The Continuum Theory of Lattice Defects," *Solid State Physics*, vol. III, eds. Seitz, F. and Turnbull, D., Academic Press, 1956.

2. Eshelby, J.D., "The Energy Momentum Tensor in Continuum Mechanics," *Inelastic Behavior of Solids*, ed. Kanninen, M.F. et al., McGraw-Hill, New York, 1970.

3. Rice, J.R., "A Path Independent Integral and Approximate Analysis of Strain Concentration by Notches and Cracks," *Journal of Applied Mechanics*, vol. 35, 1968, pp. 379-386.

4. Rice, J.R., "Mathematical Analysis in the Mechanics of Fracture," *Fracture: An Advanced Treatise*, vol. II, ed. Liebowitz, H., Academic Press, New York, 1968, pp. 191-311.

5. Rice, J.R. and Rosengren, G.F., "Plane Strain Deformation Near a Crack Tip in a Power-Law Hardening Material," *Journal of the Mechanics and Physics of Solids*, vol. 16, 1968, pp. 1-12.

6. Hutchinson, J.W., "Singular Behaviour at the End of a Tensile Crack in a Hardening Material," *Journal of the Mechanics and Physics of Solids*, vol. 16, 1968, pp. 13-31.

7. Shih, C.F., "Small Scale Yielding Analysis of Mixed Mode Plane Strain Crack Problems," ASTM STP 560, 1974, pp. 187-210.

8. Shih, C.F., "Relationships Between the J-integral and the Crack Opening Displacement for Stationary and Extending Cracks," *Journal of the Mechanics and Physics of Solids*, vol. 29, 1981, pp. 305-326.

9. Rice, J.R., "Stresses Due to a Sharp Notch in a Work-Hardening Elastic-Plastic Materials Loaded by Longitudinal Shear," *Journal of Applied Mechanics*, vol. 34, 1967, pp. 287-298.

10. McMeeking, R.M., "Finite Deformation Analysis of Crack-Tip Opening in Elastic-Plastic Materials and Implications for Fracture," *Journal of the Mechanics and Physics of Solids*, vol. 25, 1977, pp. 357-381.

11. Rice, J.R. and Sorenson, E.P., "Continuing Crack-Tip Deformation and Fracture for Plane-Strain Crack Growth in Elastic-Plastic Solids," *Journal of the Mechanics and Physics of Solids*, vol. 26, 1978, pp. 163-186.

12. Drugan, W.J., Rice, J.R. and Sham, T.L., "Asymptotic Analysis of Growing Plane Strain Tensile Cracks in Elastic-Ideally Plastic Solids," *Journal of the Mechanics and Physics of Solids*, vol. 30, 1982, pp. 447-473.

13. Rice, J.R., "Limitations to Small-Scale Yielding Approximation for Crack Tip Plasticity," *Journal of the Mechanics and Physics of Solids,* vol. 22, 1974, pp. 17-26.

14. Barsoum, R.S., "Triangular Quarter-Point Elements as Elastic and Perfectly-Plastic Crack Tip Elements," *International Journal for Numerical Methods in Engineering*, vol. 11, 1977, pp. 85-98.

15. Stern, M., "Families of Consistent Conforming Elements with Singular Derivative Fields," *International Journal for Numerical Methods in Engineering*, vol. 14, 1979, pp. 409-421.

16. Carka, D., Mear, M.E. and Landis, C.M., "The Dirichlet-to-Neumann Map for Two-Dimensional Crack Problems," *Computer Methods in Applied Mechanics and Engineering*, in preparation 2010.

17. Givoli, D. and Keller, J.B., "A Finite Element Method for Large Domains," *Computer Methods in Applied Mechanics and Engineering*, vol. 76, 1989, pp. 41-66.

18. Givoli, D. and Rivkin, L., "The DtN Finite-Element Method for Elastic Domains with Cracks and Re-entrant Corners," *Computers and Structures*, vol. 49, 1993, pp. 633–642.

19. Hilton, P.D. and Hutchinson, J.W., "Plastic Intensity Factors for Cracked Plates," *Engineering Fracture Mechanics*, vol. 3, 1971, pp. 435-451.

20. Landis, C.M., "A New Finite-Element Formulation for Electromechanical Boundary Value Problems," *International Journal for Numerical Methods in Engineering*, vol. 55, 2002, pp. 613-628.

21. Li, F.Z., Shih, C.F. and Needleman, A., "A Comparison of Methods for Calculating Energy Release Rates," *Engineering Fracture Mechanics*, vol. 21, 1985, pp. 405-421.

22. Rice, J.R. and Tracey, D.M., "Computational Fracture Mechanics," *Numerical and Computer Methods in Structural Mechanics*, Academic Press, New York, 1973, pp. 585-623.

23. Du, Z.Z. and Hancock, J.W., "The Effect of Non-Singular Stresses on Crack-Tip Constraint," *Journal of the Mechanics and Physics of Solids*, vol. 39, 1991, pp. 555-567.

24. Levy, N., Marcal, P.V., Ostergren, W.J. and Rice, J.R., "Small Scale Yielding Near a Crack in Plane Strain: A Finite Element Analysis," *International Journal of Fracture*, vol. 7, 1971, pp. 142-156.

25. Hutchinson, J.W., "Fundamentals of the Phenomenological Theory of Non-Linear Fracture Mechanics," *Journal of Applied Mechanics*, vol. 50, 1983, pp. 1042-1051.